PFG 2011 / 2, 071 – 079
Stuttgart, March 2011

Article

Geometric Property of Large Format Digital Camera DMC II 140

Karsten Jacobsen, Hannover

Keywords: Digital camera, geometry, large format CCD, systematic image errors

Summary: The *geometric property of large format digital camera DMC II 140* from Intergraph Z/I Imaging with 140 megapixels has been evaluated. This new camera is equipped with just one very large format CCD-array for the panchromatic band. The monolithic large format CCD does not require any stitching, enhancing the system accuracy. Test flights in three height levels with 5.7 cm up to 20.2 cm ground sampling distance (GSD) have been used for accuracy analysis of this camera. Very small systematic image errors confirm the excellent camera geometry. The root mean square differences at independent check points for the geometric critical height in the range of 0.7 GSD corresponds to the good image geometry.

Zusammenfassung: Die *geometrischen Eigenschaften der großformatigen Digitalkamera DMC II 140* von Intergraph Z/I Imaging mit 140 Megapixeln wurde untersucht. Diese neue Kamera ist für das panchromatische Bild mit nur einem sehr großen CCD-Sensor ausgestattet. Das homogene großformatige CCD erfordert keine Zusammenfassung von Teilbildern, was die Genauigkeit steigert. Bildflüge mit drei verschiedenen Flughöhen, entsprechend 5.7 cm bis 20.2 cm Objektpixelgröße, wurden für die Genauigkeitsanalyse der Kamera verwendet. Sehr kleine systematische Bildfehler bestätigen die ausgezeichnete Kamerageometrie. Die Quadratmittel der geometrisch kritischen Höhendifferenzen an unabhängigen Vergleichspunkten von 0,7 Objektpixeln entsprechen der guten geometrischen Bildqualität.

1 Introduction

When the first large format digital cameras have been introduced, the dream of photogrammetrists was to replace the aerial film by one large CCD-array. This was not possible at those time and so large format digital system cameras, as the DMC (Intergraph Z/I Imaging) and UltraCam (Microsoft Photogrammetry, Vexcel Imaging), based on a group of CCD-arrays, have been built. This changed now; with the new large format CCD-arrays from DALSA 140 and 250 Mega pixels are available. The problems of slow frame rate and price/performance ratio have been solved. But it is also the question, how many pixels are required for the information contents included in a 230 mm × 230 mm photo. The first simple estimations where based on the operational resolution of 40 line pairs per mm and that one line pair should be presented by two pixels, leading to 18400² pixels. Very fast it was recognized that this was not the correct manner for the comparison of the information contents because of the quite better contrast and lower noise of digital images. A comparison of details which could be extracted for topographic mapping from DMC, UltraCAM and ADS40 images as well as scanned aerial photos having different ground sampling distance (GSD), was leading to the result, that just 8520² pixels are required for the information contents of scanned aerial photos in relation to original digital images not degraded by lower effective resolution (Jacobsen 2009). This does not mean, that photos should be scanned with 27 µm pixel size; under operational conditions 18 µm pixel size is satisfying but it allows the same object identification as original digital images with 1.5 times larger object pixel size. Beside the information contents, the geometric property of digital images is important.

www.schweizerbart.de
DOI: 10.1127/1432-8364/2011/0074
1432-8364/11/0074 $ 2.25

The high geometric potential of original digital images has been demonstrated by the camera test of the German Society of Photogrammetry, Remote Sensing and Geoinformation (Jacobsen et al. 2010). But not only the accuracy potential of block adjustment with self calibration, also the image geometry, presented by systematic image errors – the difference between perspective geometry and real image geometry –, has to be taken into account influencing the model handling, especially the height determination in stereo models. In addition the reliability of stitching multi sensor images operated in UltraCam syntopic mode under rough flight conditions should be guaranteed, what is not always the case. Under syntopic imaging we understand the use of a small difference in time of imaging to have the same projection center in space for any sub-camera of a camera systems with optics aligned in flight direction (Leberl & Gruber 2003).

The convergent arrangement of the first generation DMC four panchromatic sub-cameras allows a three-dimensional stitching by bundle solution. The stitching of the four in the same plane arranged sub-cameras with in total nine sub-images of the UltraCAM is quite more complex and as recent solution by the so called "monolithic stitching" the nine panchromatic sub-images are stitched to the homogenous geometry of the lower resolution green channel, solving some existing problems (Ladstädter et al. 2010). Even if improved and more reliable, the stitching to a lower resolution reference image is not the optimal solution and is contradict to the syntopic mode because of the offset of the optics of the green channel across the flight direction. But in reality the offset of the projection centers from the synthetic projection center never plaid a remarkable role.

All the problems of stitching the high resolution panchromatic sub-images do not exist if just one homogenous CCD-array is used. Of course the flatness of the large size CCD has to be guaranteed – this is not always the case for mid-format, partially also small format CCDs, where special additional parameters had to be introduced to support especially the geometry within the image corners (Jacobsen et al. 2010 and Fig. 3).

2 DMC II

With the introduction of the DMC II 140 in 2010 the real monolithic geometry is now available for the high resolution panchromatic channel. The DMC II 140 uses the new developed DALSA 140 Megapixel CCD, but this is not the end of the development. Now DALSA started with the production of a 252 Megapixel CCD. This is used in the DMC II 230. The existing optics of the DMC II cannot use the full size of the CCD, only 230 megapixels are active and so a new optics is under develoment at Carl Zeiss and shall be available in spring 2011 for the DMC II 250 (Tab. 1).

3 Test Flights with DMC II 140

For analyzing the geometric property of the DMC II 140, flights have been made over test field Aalen, Germany with 71 targeted control points having 2 cm up to 3 cm standard deviation in all three coordinate components. The test flights with 5.7 cm and 9.5 cm GSD have approximately 65% end lap (p) and side lap (q) together with crossing flight lines having the same overlap. Only the flight with 20 cm GSD has approximately 80% end lap and side lap and also crossing flight lines (Fig. 1). The

Tab. 1: Technical data of the DMC II versions with base–to–height–relation for 60% end lap.

Camera	number of pixels	focal length	pixel size	frame rate	b/h (p=60%)	GSD at h=1000 m	relation pan/MS
DMC II 140	12096 × 11200	92 mm	7.2 µm	2 sec	0.35	7.8 cm	1 : 2.0
DMC II 230	15104 × 14400	92 mm	5.6 µm	1.7 sec	0.35	6.1 cm	1 : 2.5
DMC II 250	17216 × 14656	112 mm	5.6 µm	1.7 sec	0.29	5.0 cm	1 : 3.2

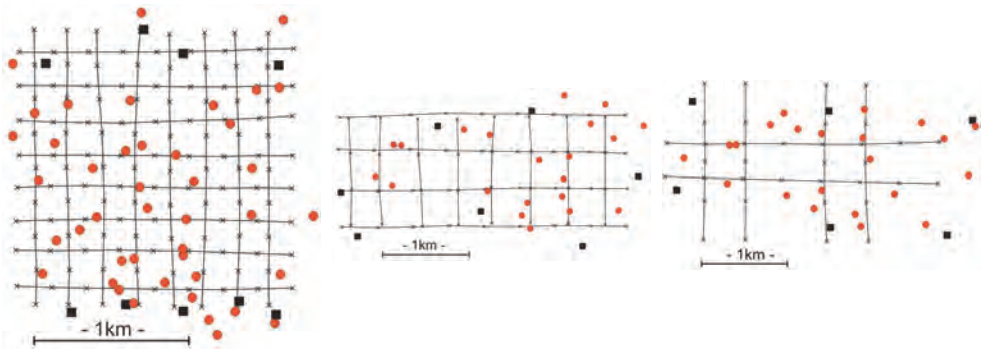

Fig. 1: Flight lines, control points (squares) and check points (red circles) of test flights; Left: 5.7 cm GSD, center: 9.5 cm GSD, right: 20.2 cm GSD.

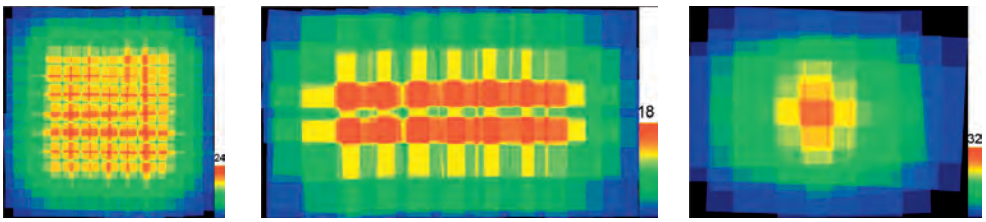

Fig. 2: Color coded overlap of images; left: 5.7 cm GSD – up to 24 images/point; center: 9.5 cm GSD – up to 18 images/point; right: 20.2 cm GSD – up to 32 images/point.

strong overlap is shown in Fig. 2. The flight conditions with sun elevations of 20° up to 25° and parts of remaining snow have not been optimal. Some control and check points have low contrast and in the flight with 20.2 cm GSD not all points could be identified.

The automatic aerial triangulation was made with ISAT. As control and check points man holes and targeted points are used. The object points have been measured in the first image where they appeared manually and in the other images by matching to the sub-matrix of the first image if possible. Only the panchromatic images have been investigated.

4 Image Geometry

The image geometry can be determined by bundle block adjustment with self calibration by additional parameters. Systematic image errors computed by bundle block adjustment show only the geometric effects which can be expressed by the used set of additional parameters; this requires also the analysis of the bundle block adjustment residuals – the remaining image coordinate discrepancies. If all residuals are overlaid corresponding to their image position and averaged in image sub-areas, then this indicates the systematic image errors which have not been covered by the used set of additional parameters. The mean value of in the average 26 up to 53 residuals in the used 225 or 625 sub-areas shows only the systematic component, while the random component of the residuals is nearly eliminated by averaging. This can be seen in Fig. 7 where the vectors are computed independently, but neighbored vectors are strongly correlated.

The CCD of the DMC II 140 has a size of 80.6 mm × 87.1 mm. The sigma0 of the bundle block adjustments are below 1 µm and the remaining systematic image errors, determined by the residuals, are clearly below 0.5 µm. In the image corner the view direction is 32.8°, requiring a flatness of the CCD below 1µm. From own experience and discussions with manufactures this is nearly impossible, but it can be determined by a calibration and respected during the image generation process.

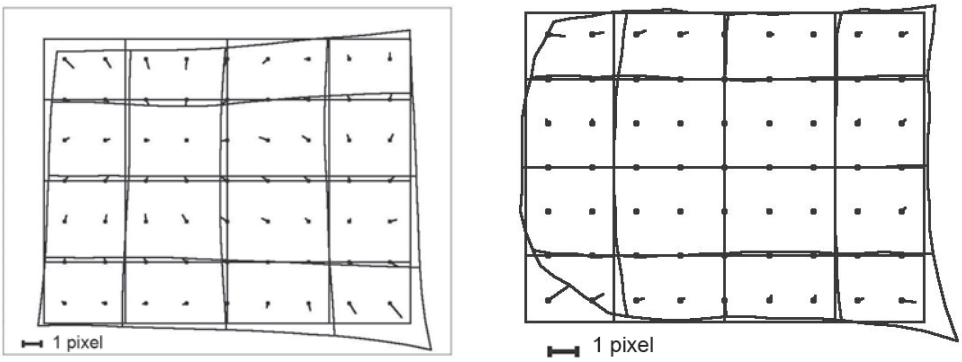

Fig. 3: Systematic image errors of a digital mid–format (36.8 mm × 49.2 mm, 6.8 µm pixel size) and a digital small–format (5.7 mm × 4.3 mm, 1.8 µm pixel size) camera (not Z/I Imaging and Vexcel Imaging) after eliminating the effect of radial symmetric distortion.

For the user this is not visible and only improved images are generated. Standard mid-format cameras, sometimes also small format digital cameras, do not include such an improved camera calibration and sometimes not an optimal mounting of the CCDs, leading to deformation of image corners (Fig. 3), which only can be compensated by special additional parameters (Jacobsen et al. 2010). If CCDs are connected at the corners or glued with the whole size to the camera body, the different thermal coefficient of the CCD, usually fixed on ceramics, and the camera body may cause a deformation of the CCD.

The investigation of the data sets was made with the Hannover program system for bundle block adjustment BLUH. It has a basic set of 12 additional parameters extended by special additional parameters for the system cameras as first generation DMC and UltraCam (Jacobsen 2007) and the mentioned parameters for determining deformations of the image corners. Earth curvature and refraction correction has been taken into account before block adjustment.

With blocks having crossing flight lines systematic image errors can be determined nearly without influence of ground control points (GCP). Systematic image errors are not changing during one flight, but they may vary for different flying elevation, mainly caused by influence of the temperature. This reduces the analysis of the systematic image errors to block adjustments using all images of the three different ground resolutions separately.

Tab. 2: Technical data of block adjustments.

GSD	images	image points	average points/image	average image points/object point
5.7 cm	144	33457	232	7.5
9.5 cm	68	16656	245	6.6
20.2 cm	36	9828	273	8.0

Tab. 3: Size of systematic image errors.

	Total effect of systematic image errors		without radial symmetric compnent		radial
GSD	root mean square	maximal	root mean square	maximal	maximal
5.7 cm	0.3 µm	1.3 µm	0.1 µm	0.3 µm	1.0 µm
9.5 cm	0.2 µm	1.5 µm	0.1 µm	0.5 µm	0.6 µm
20.2 cm	0.6 µm	3.1 µm	0.2 µm	0.8 µm	2.3 µm

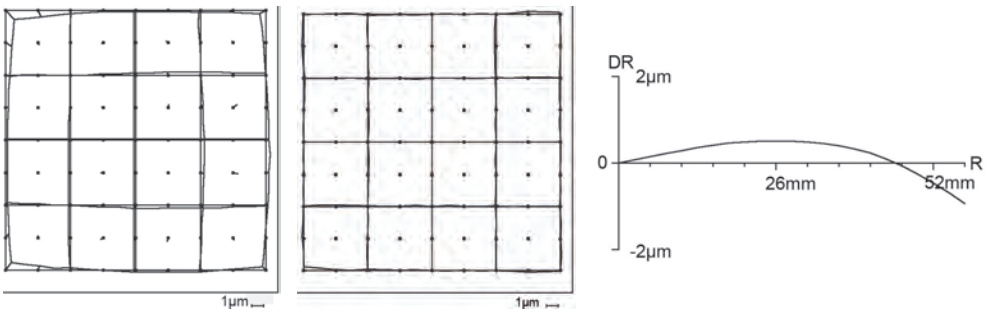

Fig. 4: Systematic image errors DMC II 140 with 5.7 cm GSD – left: whole effect, center: without radial symmetric distortion, right: radial symmetric lens distortion.

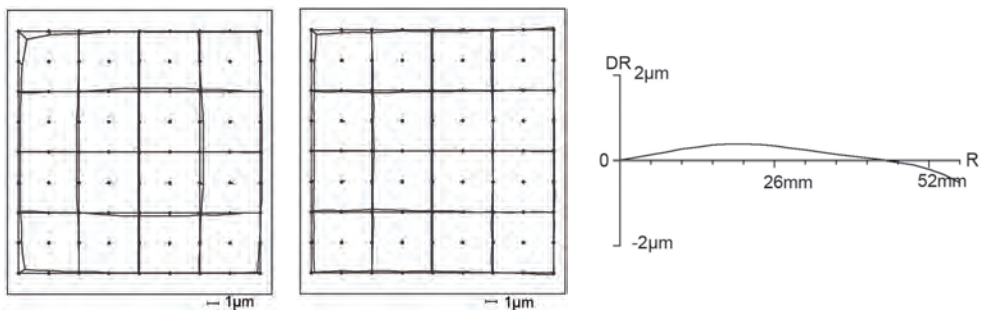

Fig. 5: Systematic image errors DMC II 140 with 9.5 cm GSD – left: whole effect, center: without radial symmetric distortion, right: radial symmetric lens distortion.

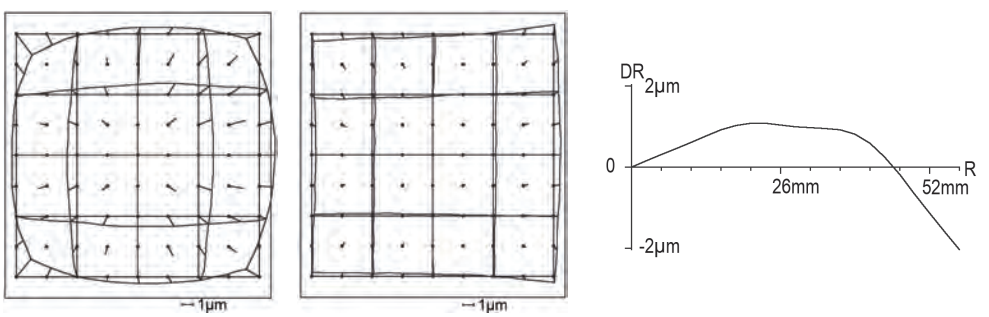

Fig. 6: Systematic image errors DMC II 140 with 20.2 cm GSD – left: whole effect, center: without radial symmetric distortion, right: radial symmetric lens distortion.

As shown in Figs. 4 up to 6, the systematic image errors do not change the character depending upon the flying height, only the dominating radial symmetric effect is changing. The change of the radial symmetric component with the flying height is a typical well known effect for all cameras. As with other data sets and other cameras the not radial symmetric components are larger for higher flying heights (Fig. 8). In general the root mean square systematic image errors of the DMC II 140 are very small (Fig. 8), the root mean square effect of 0.2 µm up to 0.6 µm correspond to 0.03 up to 0.08 pixels and after eliminating the radial symmetric component from the systematic errors to 0.01 up to 0.03 pixels. Even the maximal values are very small and would not cause problems during model han-

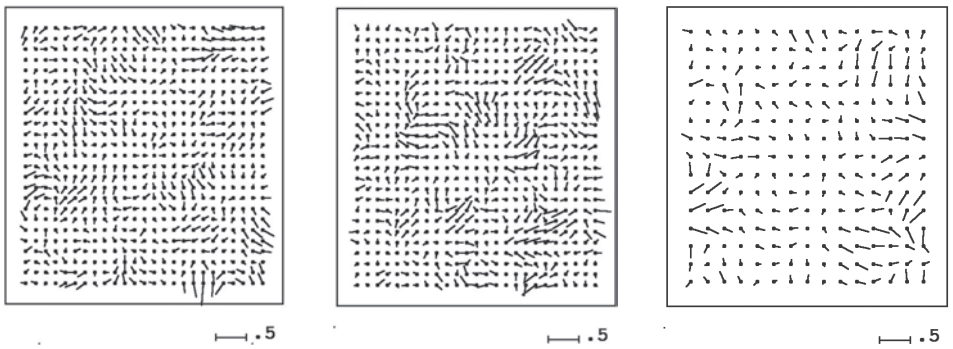

Fig. 7: Remaining systematic image errors of bundle block adjustments with self calibration by 12 additional parameters; left: related to 5.7 cm GSD; center 9.5 cm GSD; right: 20.2 cm GSD [µm].

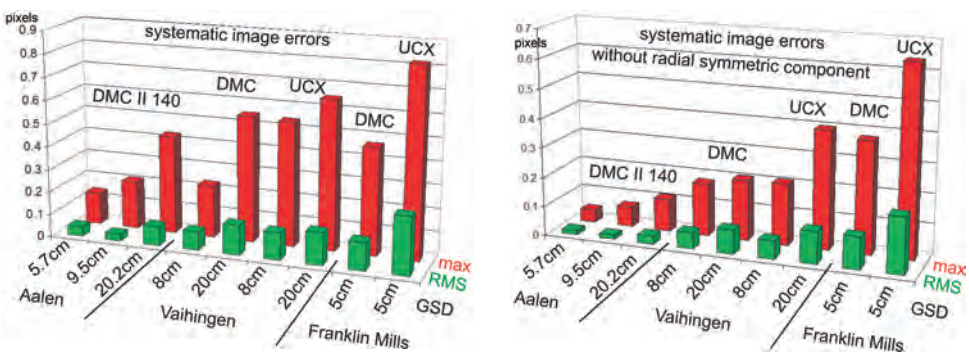

Fig. 8: Root mean square (RMS) and maximal (max) systematic image errors [pixel size] of flights over test areas Aalen, Vaihingen and Franklin Mills; Left: whole effect, right: without radial symmetric component.

dling with program systems not able to respect systematic image errors.

The analysis of the remaining systematic image errors after block adjustment with self calibration show only negligible values (Fig. 7). It is based on 33457, 16656 respectively 9828 residuals for the three different flying heights. Because of the smaller number of residuals for the 20 cm-GSD-block, the analysis for this block is reduced to 15^2 image sub-areas, while for the other blocks 25^2 sub-areas are used. In the average the individual vectors are based on 53, 26 respectively 43 residuals, causing a reduction of random errors and showing nearly only the systematic component. As root mean square size of the remaining systematic image errors after block adjustment for the 5.7 cm-GSD-block 0.14 µm (0.020 pixels), for the 9.5 cm-GSD-block 0.17 µm (0.024 pixels) and for the 20.2 cm-GSD-block 0.25 µm (0.035 pixels) is reached. Such remaining systematic image errors below 0.035 pixels are negligible and unusual small – there is no indication of any remarkable remaining systematic component. So it is not justified to improve the used set of additional parameters.

Systematic image errors of blocks flown with 60% side lap and crossing flight lines are not influenced by control points and can be compared from one test field to the other. In Fig. 8 systematic image errors of flights over the test fields Aalen, Vaihingen (Jacobsen et al. 2010) and Franklin Mills (Passini & Jacobsen 2008) are shown as fractions of the pixel size. On the left hand side of Fig. 8 the whole size and on the right hand side the systematic image errors without influence of radial symmetric component are shown. The radial symmetric component is dominated by the optics,

influenced by temperature gradiant. So the systematic image errors without the radial symmetric component represent the image geometry including stitching effects of system cameras. The comparison of the DMC II 140 with the first generation DMC and the UltraCam X demonstrate the small size of systematic image errors of the DMC II 140. The information about the also used analog cameras in the test fields Vaihingen and Franklin Mills are not included in this presentation because they are two to four times larger as the largest value shown in Fig. 8. Similar it is with the mid–format cameras AIC and DigiCam.

5 Object Point Accuracy

Bundle block adjustments using the Hannover program system BLUH with six to eight GCPs (Fig. 1) have been made with all block configurations. The block configuration did not require a support by GPS/IMU. Depending upon the data set between 48 and 19 check points have been used for the quality analysis (Fig. 1). The complete blocks with crossing flight lines and side laps in the range of 60% (fourfold blocks) are very stable, but they are not presenting the usual coverage of operational blocks. For being more realistic, also blocks only with flight lines in one direction (double blocks) and blocks only with flight lines in one direction and 24% up to 37% side lap (single blocks) have been handled. The block adjustments have bean computed without self calibration, with self calibration using the standard set of 12 additional parameters of BLUH (Jacobsen 2007) and with the standard set together with the eight special additional parameters for improving the image corners (parameters 81 up to 88) (Jacobsen et al. 2010). Program system BLUH is automatically reducing the number of additional parameters to the required set based on a combination of T-test, correlation coefficient and total correlation. So even if the following tables are listing 12 or 20 additional parameters, only a reduced number of this has been used in the final iteration.

The bundle block adjustments of the test blocks flown with the DMC II 140 with 5.7 cm, 9.5 cm and 20.2 cm GSD show very good results, but some limitations are caused by the test field. The a priori standard deviation of the control and check point coordinate components are in the range of 2 cm up to 3 cm and this is the accuracy achieved with the X- and Y-coordinates of the flight with 5.7 cm GSD. It explains why for this resolution the number of images used for the block adjustments do not have any influence to the X- and Y-component (Figs. 9 and 12). The vertical accuracy should be not as good as the horizontal, but this is re-

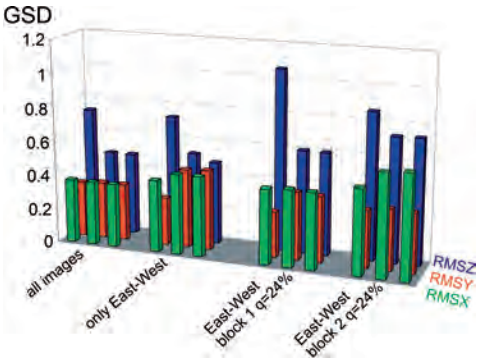

Fig. 9: Bundle block adjustments with 5.7 cm GSD, root mean square differences at check points, left columns: without additional parameters, center column: additional parameters 1 – 12, right hand column: additional parameters 1 – 12 + 81 – 88. Whole block with 144 images, with p=q=65% 72 images, with q=37% 36 images.

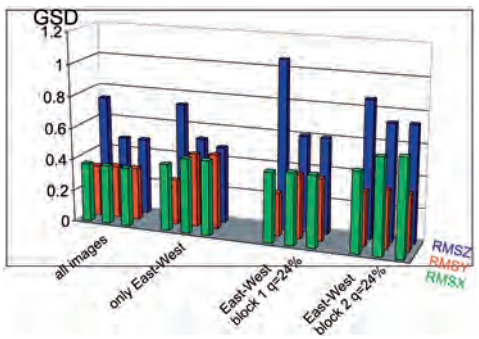

Fig. 10: Bundle block adjustments with 9.5 cm GSD, root mean square differences at check points, left columns: without additional parameters, center column: additional parameters 1 – 12, right hand column: additional parameters 1 – 12 + 81 – 88. Whole block with 68 images, only East–West 34 images, with q=34% 17 images.

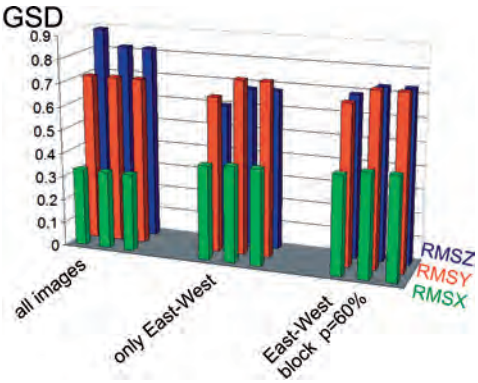

Fig. 11: Bundle block adjustments with 20.2 cm GSD, root mean square differences at check points, left columns: without additional parameters, center column: additional parameters 1 – 12, right hand column: additional parameters 1 – 12 + 81 – 88. Whole block with 36 images, only East–West 18 images, only East–West with p=60% 9 images.

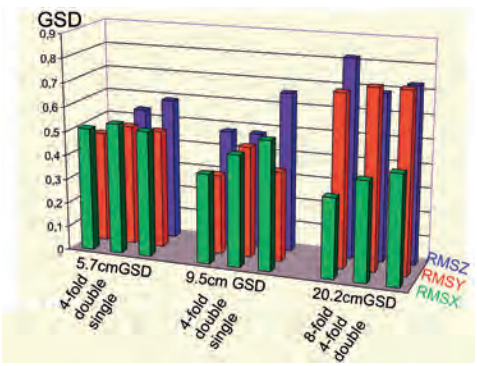

Fig. 12: Comparison of root mean square differences at check points of block adjustments with self calibration.

verse for the 5.7 cm-GSD-block using all images – indicating the limitation by the check point accuracy. The influence of the self calibration and the number of used images can be seen for the height values of the 5.7 cm-GSD-blocks and the blocks with 9.5 cm GSD. There is no advantage of the special additional parameters 81 – 88 improving the image corners. Caused by the high number of images per point, the influence of the check point accuracy and the limited size of not radial symmetric systematic image errors, the reached object point accuracy can be achieved with just the three radial symmetric additional parameters of program BLUH.

The 9.5 cm-GSD-block shows more clearly the dependencies of the root mean square discrepancies at independent check points (Fig. 10). The self calibration, at least with the radial symmetric parameters, is required for the height, but because of the very small systematic image errors it has no influence to the horizontal components. Of course the results achieved with all images are better than with just a subset of images, but as usual for test blocks with changing control point combinations, the reached accuracy relations are more close to 1.0 as corresponding to the theory that with more images a clearly better object point accuracy should be reached.

Under the not optimal flight condition, the ground resolution of 20.2 cm is too large for the available targets in the test area Aalen. Some control and check points could not be identified and the exact identification of the other was difficult (Fig. 11). By this reason the root mean square differences achieved with the 20.2 cm-GSD-block cannot be used for quality estimation, nevertheless this is not influencing the analysis of the systematic image errors. By simple theory the accuracy determined at check points should be independent upon the ground resolution, but Fig. 12 demonstrates the dependency of the results upon the test field itself, caused by the accuracy of the check point coordinates and difficulties of target identification.

6 Conclusion

The advantage of a monolithic CCD for the image geometry of the DMC II 140 is obvious. With the exception of very small radial symmetric image errors, slightly changing with the flying height, the systematic image errors are nearly negligible and smaller as for other cameras. This leads to a remarkable accuracy level of the block adjustments. In general the root mean square height differences at check points, even for single blocks, in the range of 0.7 GSD and better is excellent for a camera with a base to height relation (b/h) for 60% end lap of 0.35 or h/b=2.8. The root mean square differences in X and Y are not corre-

sponding to the vertical root mean square differences divided by 2.8 caused by the more complex situation of blocks with stronger image overlap and the limitations of the test field itself. Nevertheless the reached root mean square differences at check points for X and Y in the range of 0.4 up to 0.5 GSD is still very good. This leads to promising expectations for the DMC II 230 and 250.

References

Jacobsen, K., 2007: Geometric Handling of Large Size Digital Airborne Frame Camera Images. – Optical 3–D Measurement Techniques VIII, ETH Zürich **2007:** 164–171.

Jacobsen, K., 2009: Potential of large format digital aerial cameras. – Map World Forum, Hyderabad, GIS Development; www.gisdevelopment.net/technology/emerging/mwf09_Karsten_AerialCameras.htm (Dec. 14th 2010).

Jacobsen, K., Cramer, M., Ladstädter, R., Ressl, C. & Spreckels, V., 2010: DGPF project: Evaluation of digital photogrammetric camera systems – geometric performance. – PFG **2/2010:** 83–97.

Leberl, F. & Gruber, M., 2003: Flying the New Large Format Digital Aerial Camera Ultracam. – Photogrammetric Week **2003:** 67–76.

Ladstädter, R., Gruber, M. & Wiechert, A., 2010: Monolithic Stitching: One sensor geometry for multiple sensor camera. – ASPRS 2010 Annual Conference San Diego.

Passini, R. & Jacobsen, K., 2008: Geometric Analysis on Digital Photogrammetric Cameras. – ASPRS 2008 Annual Conference Portland.

Address of the Author:

Dr.-Ing. Karsten Jacobsen, Leibniz Universität Hannover, Institut für Photogrammetrie und Geoinformation, Nienburger Str. 1, D–30167 Hannover, Tel.: +49–511–762-2485, Fax: -2483, e–mail: jacobsen@ipi.uni–hannover.de

Manuskript eingereicht: November 2010
Angenommen: Januar 2011